

$Ce^{3+}:Na^+$ pairs in CaF_2 and SrF_2 : Absorption and laser-excitation spectroscopy, and the observation of hole burning

Dee William Pack,* William J. Manthey,[†] and Donald S. McClure
Department of Chemistry, Princeton University, Princeton, New Jersey 08544

(Received 3 April 1989)

Optical evidence of multiple $Ce^{3+}:Na^+$ charge-compensation sites in codoped $Ce^{3+}:Na^+:CaF_2$ and $Ce^{3+}:Na^+:SrF_2$ crystals is reported. High-resolution absorption and laser-excitation spectroscopy reveal the presence of numerous lines in the 32 200–32 400-cm⁻¹ region indicating a quasirandom distribution of pair sites. The absorption spectra of annealed $Ce^{3+}:CaF_2$ and $Ce^{3+}:Na^+:CaF_2$ crystals reveal isolated O_h lines. This fact has aided the interpretation of the $Ce^{3+}:Na^+$ pair spectra. Evidence for photoionization of charge-compensated Ce^{3+} sites followed by trapping of the electron at remotely compensated (O_h) Ce^{3+} sites is presented. Acceptor-type hole burning, the disappearance of the cubic Ce^{3+} site's absorption line while exciting the $Ce^{3+}:Na^+$ pair centers, is observed in both CaF_2 and SrF_2 hosts. The holes persist for weeks after their creation and survive thermal cycling to room temperature.

I. INTRODUCTION

Trivalent rare-earth ions are readily soluble in the alkaline-earth fluorides CaF_2 and SrF_2 . They enter substitutionally at the Ca^{2+} and Sr^{2+} sites. The extra positive charge of the rare-earth relative to the ion it replaces makes some type of charge-compensation mechanism necessary, either remote or local. The presence of a particular type of site in a given crystal sample depends on the growth environment and the thermodynamic and kinetic behavior of the ions in the melt and solid sample. Ce^{3+} is an attractive ion with which to investigate the charge-compensation question with optical techniques since, having the simple electron configuration $4f^1$, its sites exhibit simple spectra. Several types of Ce^{3+} charge-compensation centers in fluorite structure lattices have been identified. Two common sites for Ce^{3+} (and for the other trivalent rare-earth ions) are the tetragonal center, $C_{4v} F^-(100)$, where a fluorine ion resides in the nearest interstitial lattice site, and the trigonal center, $C_{3v} O^{2-}(\frac{1}{2}\frac{1}{2}\frac{1}{2})$, where an oxygen ion replaces a fluoride in the cube surrounding the rare-earth ion. In crystals grown in the absence of oxygen the former predominates. The charge-compensator coordinates are expressed in the crystallographic (hkl) notation in units of $\frac{1}{2}$ the unit-cell dimension, a_0 . $\frac{1}{2}a_0$ is the distance between adjacent body-centered sites in the fluorite lattice. Kaplyanskii *et al.*¹ have published optical-absorption and emission spectra of the $Ce^{3+} C_{4v} F^-(100)$ site in CaF_2 , SrF_2 , and BaF_2 and also the $Ce^{3+} C_{3v} O^{2-}(\frac{1}{2}\frac{1}{2}\frac{1}{2})$ center in CaF_2 . Not all of the predicted energy levels were observed in this early work. Manthey^{2,3} has completed a detailed study of the $Ce^{3+} C_{4v} F^-$ center including a full crystal-field-theory treatment. He also reports some additional information on the two trigonal Ce^{3+} center absorption lines, $C_{3v} O^{2-}(\frac{1}{2}\frac{1}{2}\frac{1}{2})$ and $C_{3v} F^-(111)$. Magnetic susceptibility and infrared absorption measurements aimed at establishing the energies of the ground state $4f$ manifold

for the $C_{4v} F^-(100)$ site in CaF_2 and SrF_2 have been published by Mires and Walker.^{4,5} Freeth and Jones⁶ have completed additional infrared measurements and energy-level modeling work on this site in the two hosts. Jacobs *et al.*⁷ have published a detailed study of the electronic and vibrational spectra of $Ce^{3+} C_{4v} X^-(100)$ sites in CaF_2 and SrF_2 , when X^- was the H^- , D^- , or T^- ion. Pre-1974 optical data, as well as pertinent magnetic experiments, have been summarized in Ref. 8. Theoretical analyses have been completed by Manthey^{2,3} and Starostin and co-workers⁹ on energy-level and line-intensity data for the $C_{4v} F^-(100)$ site. The latter authors also have completed similar work for some of the alternative centers,¹⁰ including the $C_{2v} Na^+(110)$ and the O_h site, for which no optical data existed until the present study.

A new class of charge-compensation sites may be created by doping monovalent impurity ions along with trivalent rare-earth ions into fluorite hosts. The charge balance is preserved by the substitution of the monovalent ion at a divalent calcium site, thus providing a net negative charge. ESR evidence for the existence of these types of sites has previously been reported.^{11,12} The monovalent ion chosen for codoping with Ce^{3+} into the CaF_2 and SrF_2 host lattices is Na^+ . The ionic radius match to Ca^{2+} , and Sr^{2+} is fairly close [$r(Na^+)=1.06 \text{ \AA}$, $r(Ca^{2+})=1.02 \text{ \AA}$, $r(Sr^{2+})=1.18 \text{ \AA}$],¹³ and NaF has been found to dissolve by prior workers.¹¹

The first 24 $Ce^{3+}:Na^+$ sites are listed in Table I with the Ce^{3+} ion as the origin, and the coordinates of the Na^+ compensator given in units of $\frac{1}{2}a_0$, where a_0 is the lattice constant (for CaF_2 , $a_0=5.4629 \text{ \AA}$ at room temperature; for SrF_2 , $a_0=5.7996 \text{ \AA}$ at room temperature⁸). Table I also contains the $Ce^{3+}-Na^+$ separation and the number of equivalent orientations for each site. The Na^+ substitutional sites [(110), (200), etc., the even sublattice] are indexed by the integer n related to the coordinates and distance by $h^2+k^2+l^2=2n=R^2$.¹⁴

Figure 1 shows idealized pictures of the $C_{4v} F^-(100)$

TABLE I. Ce³⁺:Na⁺ pair sites in the fluorite lattice. a_0 is the lattice constant.

n	(hkl) $(\frac{1}{2}a_0 \text{ units})$	$R = \frac{1}{2}(2n)^{1/2}$ $(a_0 \text{ units})$	Symmetry	Number of equivalent sites
1	110	0.71	C_{2v}	12
2	200	1.00	C_{4v}	6
3	211	1.22	C_s	24
4	220	1.41	C_{2v}	12
5	310	1.58	C_s	24
6	222	1.73	C_{3v}	8
7	321	1.87	C_1	48
8	400	2.00	C_{4v}	6
9	330	2.12	C_{2v}	12
9	411	2.12	C_s	24
10	420	2.24	C_s	24
11	332	2.35	C_s	24
12	422	2.45	C_s	24
13	431	2.55	C_1	48
13	510	2.55	C_s	24
15	521	2.74	C_1	48
16	440	2.83	C_{2v}	12
17	433	2.92	C_s	24
17	530	2.92	C_s	24
18	442	3.00	C_{2v}	12
18	600	3.00	C_{4v}	6

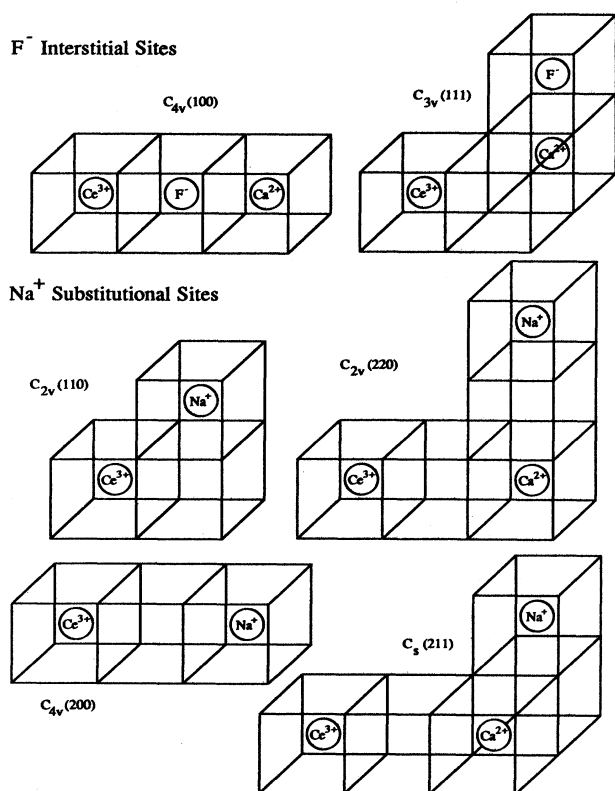


FIG. 1. Model pictures of some Ce³⁺ charge-compensation pairs. Examples of both the Na⁺ substitutional sites and the F⁻ interstitial sites are shown.

and C_{3v} F⁻(111) sites, and also of the first four Ce³⁺:Na⁺ sites. CaF₂ and SrF₂ samples codoped with low concentrations of CeF₃ (0.003–0.006 mol %) and an excess of NaF (0.1 mol %) exhibit many new lines in their low-temperature, ultraviolet spectra. The appearance of these spectra immediately suggests the coexistence of many of these Ce³⁺:Na⁺ charge-compensation sites. No one line, or group of lines, dominates in intensity. The distribution present in the samples appears to be random, based on site occurrence, rather than thermodynamic, based on electrostatic site binding stability. This is in contrast to crystals with fluoride-ion interstitial sites where the optical evidence points to the predominance of the most stable, nearest-neighbor charge-compensated sites.^{1,2}

Figure 2 shows the 4*f*, and partial 5*d*, energy-level diagram of Ce³⁺ as a free ion, in a cubic crystal field, and in a low-symmetry crystal field. The low-symmetry field diagram is representative of the charge-compensation centers studied. The degenerate 4*f* *G* states, and the 5*d* *e* level, are split by the axial fields (this splitting is somewhat exaggerated in Fig. 2). The ²F_{7/2} and ²F_{5/2} states split into five levels in the cubic field, and seven in a lower-symmetry environment (C_{4v} , C_{3v} , C_{2v} , etc.). The 4*f* spin-orbit splitting of the Ce³⁺ impurity does not change much from the free-ion value, 2253 cm⁻¹.¹⁵ Spin-orbit coupling in the 5*d* levels is omitted from Fig. 2. Only the sharp transitions between the 4*f* manifold and the 5*d* *e* levels are considered in this study. An analysis of the broad, higher-energy 4*f* → 5*d* *t* absorption bands from the common Ce³⁺ C_{4v} F⁻(100) site in CaF₂ has been completed.^{2,3}

The symmetry notation for the double-group representations of various point groups is made clear in Table II.

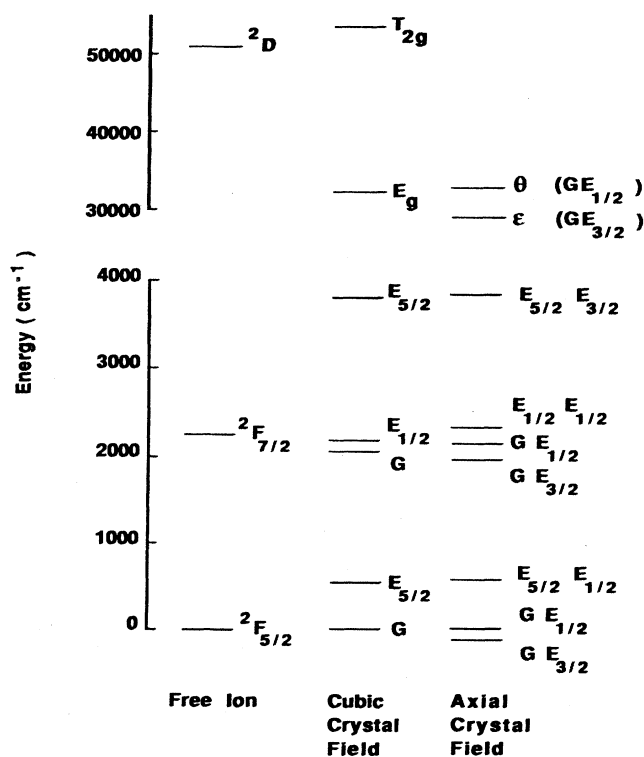


FIG. 2. The $4f, 5d$ energy-level diagram of Ce^{3+} as a free ion, in a cubic crystal field, and in a low-symmetry field. Energies are representative of the Na^+ sites studied.

The gammas are Bethe's notation. The somewhat more descriptive E and G notation is that of Mulliken as modified by Herzberg. Clear labeling of the low-symmetry representations includes the cubic parent notation. For example, the $E_{3/2}$ ground state of the Ce^{3+} ion in a C_{4v} -symmetry site is labeled $G E_{3/2}$, distinguishing it from the higher-energy $E_{5/2}E_{3/2}$ state.

The purpose of this report is to present evidence for the existence of multiple $Ce^{3+}:Na^+$ charge-composition sites in CaF_2 and SrF_2 , and to present a comprehensive set of optical data for these centers. Since we find evidence that the Ce^{3+} at these sites photoionize, the high-resolution spectroscopic data are of particular interest. Section II contains descriptions of the experimental techniques employed. Section III presents high-resolution absorption spectra of CaF_2 samples containing the O_h

TABLE II. Two common notations for the double-group representations of point groups of interest. Reduction of symmetry from O_h reads left to right.

O_h	C_{4v}	C_{3v}	C_{2v}	C_s
$E_{1/2} (\Gamma_6)$	$E_{1/2} (\Gamma_6)$	$E_{1/2} (\Gamma_6)$	$E_{1/2} (\Gamma_5)$	$E_{1/2} (\Gamma_{34})$
$E_{5/2} (\Gamma_7)$	$E_{3/2} (\Gamma_7)$	$E_{1/2} (\Gamma_6)$	$E_{1/2} (\Gamma_5)$	$E_{1/2} (\Gamma_{34})$
$G_{\pm 1/2} (\Gamma_8)$	$E_{1/2} (\Gamma_6)$	$E_{1/2} (\Gamma_6)$	$E_{1/2} (\Gamma_5)$	$E_{1/2} (\Gamma_{34})$
$G_{\pm 3/2} (\Gamma_8)$	$E_{3/2} (\Gamma_7)$	$E_{3/2} (\Gamma_4)$	$E_{1/2} (\Gamma_5)$	$E_{1/2} (\Gamma_{34})$

center, and of samples containing multiple $Ce^{3+}:Na^+$ sites. Section IV contains the laser-excitation spectra of the multiple-site CaF_2 sample, and includes the observation of persistent spectral hole burning (the disappearance of the O_h site). The spectra show evidence that the charge-compensated sites photoionize and that the remotely compensated O_h sites trap the freed electron. In Sec. V laser-excitation spectra of $Ce^{3+}:Na^+$ codoped into SrF_2 are presented and discussed. The results in this other host crystal are quite similar, including the observation of a hole in the spectrum at the O_h site, and complement the CaF_2 results. Section VI summarizes our conclusions and contains suggestions for future work. A planned companion paper¹⁶ will contain site-selective laser spectroscopic results, crystal-field theory for the cubic and Na^+ pair sites, and a discussion of the site identifications.

II. EXPERIMENTAL DETAILS

Four types of experiments were employed in the investigation of the Ce impurity centers in CaF_2 and SrF_2 . These are absorption spectroscopy,³ broad-band-monitored excitation,¹⁷ narrow-band-monitored, site-selective excitation,¹⁷ and site-selective emission.¹⁷ A brief description of the techniques and of the experimental apparatuses follows. While the results from the two-site-selective methods will be reported in the future, the rather similar experimental setups are described below.

Absorption spectra³ were taken with a Jarrell-Ash 3.4-m monochromator using a Ebert-mounted 30 000-lines/in. grating in first order. The effective resolution was about 0.5 cm^{-1} . Spectra were recorded either photoelectrically or on photographic plates. Fe-Ne and Pt-Ar hollow-cathode lamps provided calibration lines. Samples were immersed in liquid helium in a Janis Dewar equipped with a vacuum system in order to reach superfluid helium temperatures and eliminate bubbles.

For excitation and emission spectra¹⁷ a Moletron DL II dye laser equipped with a doubling crystal is used as the excitation source. The laser linewidth is 0.3 cm^{-1} , and 0.6 cm^{-1} when doubled. uv laser power is $\sim 20 \mu\text{J/pulse}$ and the laser is typically run at a repetition rate of 20 pulses/s. The experimental setup is shown in Fig. 3. During excitation scans four channels of data are gathered by gated integrators on a shot by shot basis: (1) emission signal, (2) laser-power reference, (3) 1.0-cm^{-1} étalon fringe-counting photomultiplier tube (PMT), and (4) the optogalvanic signal from an Fe-Ne hollow-cathode lamp. Optogalvanic lines are used as absolute calibration references and the étalon fringe pattern is used for relative calibration. This allows absolute calibration accuracy of better than 1 cm^{-1} , and relative calibrations (peak spacings) accurate to 0.1 cm^{-1} . Fifty shots of signal, divided by reference, are averaged and stored. The excited emission is monitored at 342 nm with the monochromator slits wide open (0.3 cm). The emission signal is monitored by an uv-sensitive, low-noise Hamamatsu R-212 photomultiplier tube. Some excitation spectra were taken without the étalon calibration pattern and were thus un-

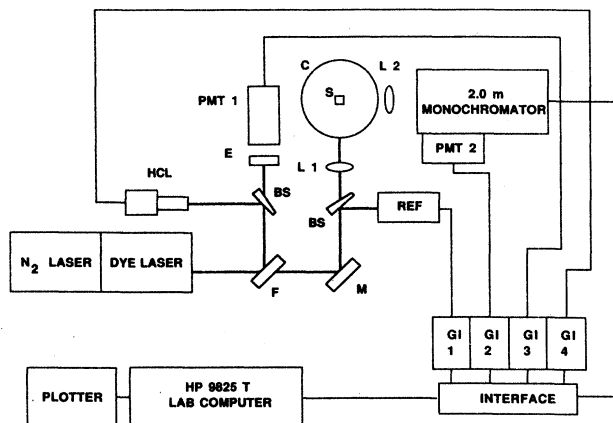


FIG. 3. High-resolution emission and excitation apparatus. *F* is the Corning 7-54 uv pass filter. *M* is the mirror. *BS* is the quartz beam splitter. *HCL* is the Fe-Ne hollow cathode lamp. *E* is the 1-cm⁻¹ free spectral range étalon. *PMT 1* is the 1P-28 photomultiplier tube fronted by a pinhole. *PMT 2* is the Hamamatsu R-212 low-noise photomultiplier tube. *C* is the cryostat. *S* is the sample crystal. *L1* is the 0.5-m-focal-length quartz lens. *L2* is the 7-cm quartz lens. *REF* is the 1P-28 PMT with MgF₂ scattering surface. The *GI* are the Stanford Research Systems, Inc. SRS-250 and Moletron LP-20 gated integrators.

corrected for laser sine drive error. These spectra were scaled by using a correction pattern from another scan, resulting in a peak position agreement of 0.3 cm⁻¹ or better between scans. For 1.8-K spectra, a custom-made Pope liquid-helium immersion Dewar is employed. A vacuum system is used to reach superfluid He temperatures. For 15±2 K (temperature at sample) spectra, an Air Products Displex closed-cycle He refrigerator is used.

For emission spectra, the 2.0-m McPherson monochromator slits are closed to 50 μm, giving an effective resolution of 3.3 cm⁻¹. The monochromator was equipped with a 1200-lines/mm grating blazed for 7000 Å, and was used in second order. Prior to each scan the monochromator was calibrated with a convenient Hg pen-lamp line (312.5663 nm). The hollow-cathode lamp and étalon plus PMT fringe-counting arrangement in Fig. 3 are removed during emission scans. As in the excitation experiments, the data are collected on a shot-by-shot basis and are normalized for laser-power fluctuations. A Displex refrigerator is used to cool the sample to 15 K.

Doubly doped Ce³⁺:Na⁺-containing crystals are prepared from CaF₂ and SrF₂ with low percentages of CeF₃ (0.020–0.003%), and larger amounts of NaF (0.100%) added. The percentages are by weight with respect to CaF₂. Carbon crucibles are covered to reduce the escape of volatilized NaF. Despite the closed crucibles, Na⁺ centers are most efficiently produced with a large excess of NaF.³ The final concentration of Na⁺ in the samples is not known, but is certainly much less than the 0.100% initially added. The CaF₂ samples were grown by H. Temple of the RCA Corporation by way of

the gradient freeze method, and were kindly donated for our use. SrF₂ samples were grown by L. DeShazer of the Hughes Corporation and kindly donated for our use by V. Nicolai of the Office of Naval Research. A brief description of the heat treatments given to some of the studied samples follows.

To produce uncompensated *O_h* centers in a Ce³⁺:CaF₂ sample, the annealing procedure of Ref. 18 was followed. Friedman and Loh¹⁸ found via ESR that CaF₂ crystals doped with Ce³⁺ and Gd³⁺, and heat treated as follows, exhibited predominantly *O_h*-site signals. Fragments of a 0.002% Ce³⁺:CaF₂ crystal (sample 1), plus powdered CaF₂, were placed in a quartz tube. The tube was heated and evacuated to out-gas unwanted oxygen. The tube was then sealed and gradually heated to 1200°C. After 12 h at that temperature it was quickly quenched in cold water. The resulting spectrum is shown in Fig. 4(a).

Some Ce³⁺:Na⁺:CaF₂ double-doped samples were similarly heat treated to produce uncompensated Ce³⁺ centers or to select against the thermodynamically favored F⁻ interstitial sites by fast cooling. The samples' heat treatments differed in the cooling rate between solidification and room temperature. Three (Ce, Na)-doped samples were cooled at different rates and, as shown in Figs. 4(b)–4(d) quite different spectra resulted. The detailed thermal treatments are not accurately known, however, and this aspect of the sample preparation has not been studied. All laser experiments on Ce³⁺:Na⁺:CaF₂ were performed on a piece of sample 4. No heat treatments were done on the Ce³⁺:Na⁺:SrF₂ samples.

III. ABSORPTION SPECTRA OF THE Ce³⁺:Na⁺:CaF₂ CHARGE-COMPENSATION PAIRS AND THE Ce³⁺ *O_h* SITE

Figure 4 shows absorption spectra³ in the 314–308-nm region from four different samples: (a) 0.001 at. % Ce³⁺:CaF₂ (sample 1), (b) 0.003 at. % Ce³⁺:0.1 at. % Na⁺:CaF₂ (sample 2), (c) 0.02 at. % Ce³⁺:0.1 at. % Na⁺:CaF₂ (sample 3), and (d) 0.003 at. % Ce³⁺:0.1 at. % Na⁺:CaF₂ (sample 4). Consider Fig. 4(a). The line at 313.17 nm is the well-studied 4*f* *G* *E*_{3/2} → 5*de* *G* *F*_{3/2} transition of the Ce³⁺ *C*_{4*v*} F⁻ site. Since the crystal was grown in the manner reported¹⁸ to yield uncompensated *O_h*-symmetry Ce³⁺ centers, the assignment of the higher-energy line at 309.23 nm [32 329 cm⁻¹, full width at half maximum (FWHM)=2.6 cm⁻¹] due to the uncompensated Ce³⁺ *O_h* site's 4*f* *G* → 5*de* *G* transition is made. This assignment is greatly strengthened by information from the spectra of Ce³⁺:Na⁺ codoped crystals discussed below and by emission results which will be reported in a future paper. Broader bands from the *C*_{4*v*} center's vibronic transitions are also present in Fig. 4(a) and other spectra. The most prominent of these is the 308.5-nm line due to the 486-cm⁻¹ vibration. This vibrational line was assigned to an *A*_{1*g*} breathing mode of the F⁻ cube surrounding the Ce³⁺ ion by Hayes *et al.*¹⁹ A strong progression in this mode occurs in Ce³⁺:CaF₂, and also in SrF₂ and BaF₂ systems at different frequencies,

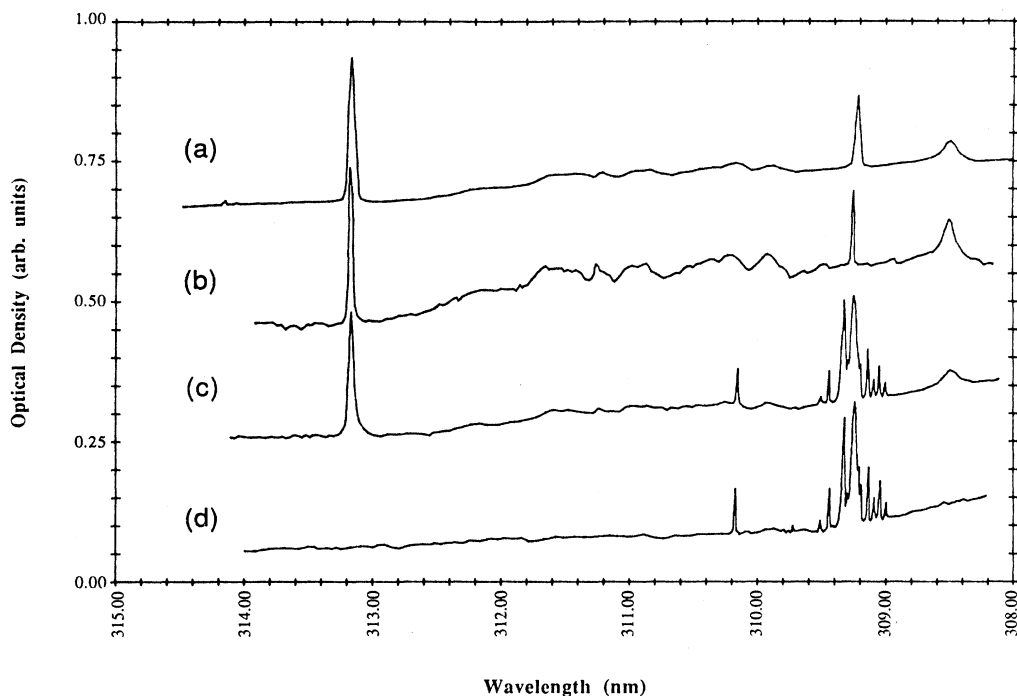


FIG. 4. 2.2-K high-resolution absorption spectra of four $\text{Ce}^{3+}:\text{CaF}_2$ samples. (a) Sample 1, 0.001 at. % $\text{Ce}^{3+}:\text{CaF}_2$, 3.1 mm, heat treated. (b) Sample 2, 0.003 at. % $\text{Ce}^{3+}:0.1$ at. % $\text{Na}^+:\text{CaF}_2$, ~ 1 mm, slow cooled. (c) Sample 3, 0.02 at. % $\text{Ce}^{3+}:0.1$ at. % $\text{Na}^+:\text{CaF}_2$, 0.18 mm. (d) Sample 4, 0.003 at. % $\text{Ce}^{3+}:0.1$ at. % $\text{Na}^+:\text{CaF}_2$, 1.1 mm, fast cooled. All spectra are digitized microdensitometer traces of photographic plates.

making its identification as a configuration coordinate a natural choice.²⁰

Figure 4(b) shows the $C_{4v} F^-$ and the O_h site's zero-phonon lines occurring in $\text{Ce}^{3+}:\text{Na}^+$ codoped sample 2, which was slowly cooled from solidification to room temperature. This procedure apparently allowed the Na^+ ions to volatilize leaving their Ce^{3+} ions at uncompensated sites. The wavelength of the O_h line is 309.25 nm (32327 cm^{-1}), slightly different from that of sample 1, but within the latter's bandwidth.

Figures 4(c) and 4(d) exhibit a thicket of lines absent in singly doped samples. Approximately a dozen lines are clustered between 309.5 and 308.9 nm, and a prominent peak appears around 310.2 nm. These are identified as zero-phonon lines from the $4f \rightarrow 5de$ transitions of $\text{Ce}^{3+}:\text{Na}^+$ charge-compensation sites. It is expected that the $5de$ level will be split by the low-symmetry crystal fields of the Na^+ compensators, each site thereby giving rise to a doublet, although one of the transitions might be weak. The observation of 12 or more prominent lines of this type indicates the presence of multiple $\text{Ce}^{3+}:\text{Na}^+$ charge-compensation sites in these samples. The existence of many Na^+ sites is interesting since only a few of the possible sites of other charge compensators, such as F^- and O^{2-} , are usually present in measurable concentration.⁸ This can be explained by the high temperature at which the distribution is frozen in and the relatively small Coulomb attraction of the trivalent ion and its charge compensators. The detailed spectral features of

the $\text{Ce}^{3+}:\text{Na}^+$ sites are more readily seen in the excitation spectra of Fig. 5. The corresponding line list is given in Table III. Note that the spectra in Figs. 4(c) and 4(d) show a broad central region centered at 309.3 nm that overlaps the position of the O_h -site line. As Na^+ ions occupy increasingly distant charge-compensation sites, the low-symmetry crystal-field splitting of the $5de$ level into its $|\epsilon\rangle(d_{x^2-y^2})$ and $|\theta\rangle(d_{z^2})$ components will shrink. In Figs. 4(c) and 4(d), well-resolved lines due to the closely spaced $\text{Ce}^{3+}:\text{Na}^+$ pairs are observed, as well as overlapping lines caused by more distant Na^+ ions. These partially resolved lines eventually form a broad region as the splittings become unresolved. These observations reinforce the assignment of the isolated line at 309.25 nm in Figs. 4(a) and 4(b) as originating from the O_h site, as it falls in the midst of the broad "distant compensation" region. The relative strength of the various Na^+ lines are independent of the Ce^{3+} doping level for the concentration range investigated.

While a full study of growth conditions and annealing treatments of these singly and doubly doped crystals would be highly desirable to elucidate the details of site formation, this would involve many more samples than available, and has not been done. Here, the few examples of the heat treatments that have been performed, which led to the different spectra shown in Fig. 4, are discussed. Several samples of $\text{Ce}^{3+}:\text{Na}^+:\text{CaF}_2$ were studied³ which exhibited low-temperature absorption spectra similar to that of sample 3 in Fig. 4(c), with the Na^+ -site lines in

the 310–309-nm region and the $C_{4v} F^-$ -center line at 313.17 nm. The $C_{4v} F^-$ center always appeared in these unannealed samples. At very high temperatures the impurity ions are expected to be mobile in the CaF_2 lattice, and the distribution of charge-compensated centers to be random and distant. Upon cooling, the ion mobility and the site stability dictated by electrostatic forces combined with entropy determine the final distribution.²¹ A rapid-

cooling treatment should freeze in the high-temperature ion distribution and lead to remotely compensated, O_h -symmetry impurity sites. This was observed for $Ce^{3+}:CaF_2$ by Friedman and Loh¹⁸ with ESR. Our similar optical result is shown in Fig. 4(a), qualified by the presence of the thermodynamically favored $C_{4v} F^-$ center as well. The doubly doped samples show a somewhat more complex annealing behavior. The slowly

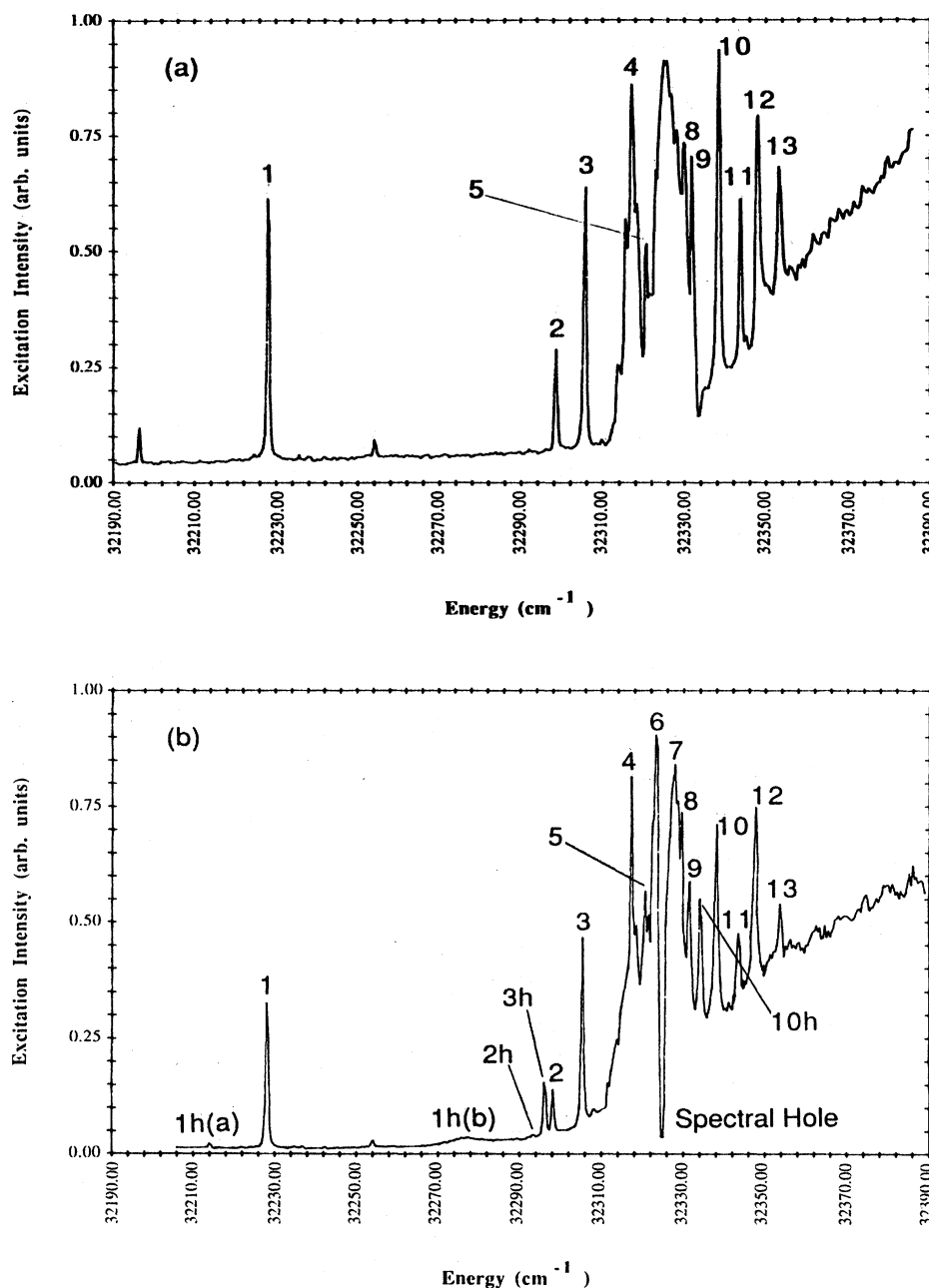


FIG. 5. High-resolution laser-excitation spectra of sample 4, $Ce^{3+}:Na^+:CaF_2$. Peak energies and features are tabulated in Table III. (a) Initial 1.8-K spectrum [this is very similar to the absorption spectrum in Fig. 4(c)]. (b) Later 15-K spectrum. Note the hot bands and the appearance of a spectral hole at 32 325 cm^{-1} . (c) 15-K spectrum after extensive laser excitation of all prominent peaks. Note the reduction of the outlying peak intensities relative to the central 32 320–32 330- cm^{-1} region.

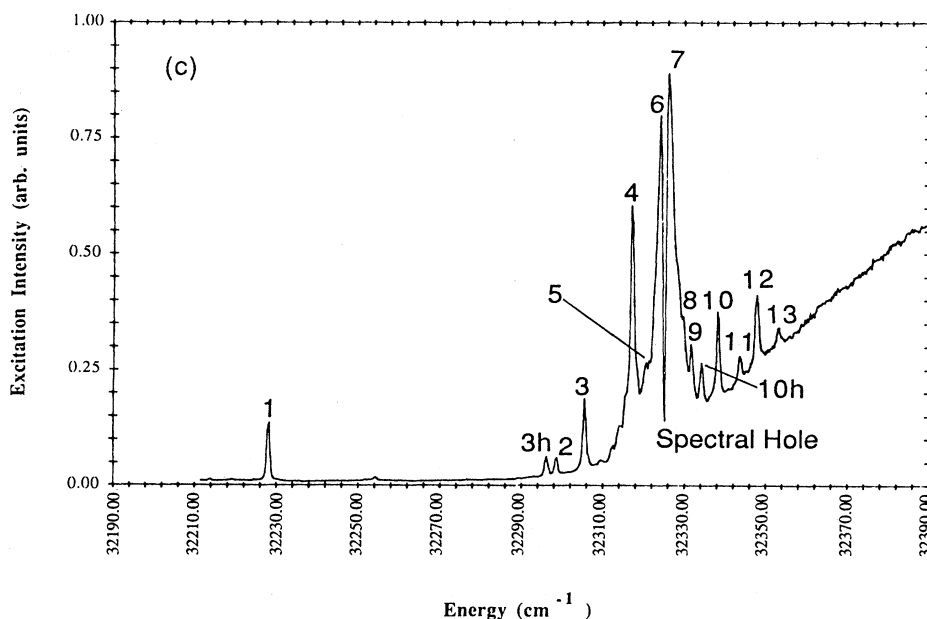


FIG. 5. (Continued).

cooled sample 2 [Fig. 4(b)] showed the only C_{4v} F^- -center line and the remotely compensated O_h line, while the rapidly cooled sample 4 [Fig. 4(d)] manifested only Na^+ sites.

Excess NaF will volatilize at temperatures near the melting point, but may first drive out the F^- compensators as in sample 4, and upon rapid cooling leave the Na-Ce pair distribution as we observe it. A statistical treatment of this distribution can be carried out assuming equilibrium at some reasonably high temperature, say $T_d = 1500$ K, below which Na^+ diffusion is slow in CaF_2 . This should lead to a population distribution n_i of the different pairs and of the distant, nearly cubic sites. The low Ce concentration of 0.003 wt. % corresponds to $x = 7.6 \times 10^{-5} M$ or approximately 1 Ce^{3+} ion per 13 000 Ca^{2+} sites. This is approximately the number of sites enclosed in a sphere of radius $9a_0$ (a_0 , the unit-cell length, is 5.46 Å for CaF_2). The formula $n \approx 4(\frac{4}{3}\pi r^3)$ is employed to get this result.²² The number n_i of each Na-Ce pair would be in a Boltzmann distribution possibly determined by the largely Coulombic attraction between Na and Ce and the statistical weight g_i of each type of pair:

$$\frac{n_i}{n_T} = \frac{g_i \exp(-u_i/kT_d)}{q},$$

where n_T is the total number of pairs and u_i is the attractive potential, provisionally given by $u_i = -e^2/\epsilon R_i$. R_i is the pair separation and ϵ , the dielectric constant, is 6.7 for CaF_2 .⁸ Here we ignore reductions in the dielectric constant which may be expected for the most closely associated pairs. For CaF_2 with a T_d of 1500 K, $u_i/kT_d = -3.04/m$, where m is the number of unit-cell lengths between paired Na and Ce ions. The partition function q has to be expressed for the sphere containing one Ce to avoid problems with the definition of pairs.

Distinct pairs cannot be resolved beyond $m = 3$, which is an order of magnitude smaller than $(1/x)^{1/3}$. Therefore, we write

$$q = \sum_{i=1}^{m \approx 3} g_i \exp\left[\frac{-u_i}{kT_d}\right] + \frac{1}{x} - \sum_{i=1}^{m \approx 3} g_i,$$

where the last term is 446, the number of Ca sites in a sphere of radius $3a_0$, and hence it can be neglected compared to $1/x$. When compared to the spectrum shown in Fig. 5(a), this result shows that the pair contribution to the partition function must depend much more on the attractive potential than on statistics, even though, as we now show, the spectrum at first looks as though it is close to that of a random distribution.

Figure 5(a) is the laser-excitation spectrum of $Ce^{3+}:Na^+:CaF_2$, sample 4, at 2 K. The laser-line width of 0.3 cm^{-1} is less than the inhomogeneous broadening of the lines. The prominent lines are numbered 1–13. Between lines 6 and 7 is a region ($32\,322\text{--}32\,328 \text{ cm}^{-1}$) which appears to be due to the near continuum of pairs having large distances of separation. Lines 1, 2, and 3 have the intensity ratios 12:5:12. Our first attempt at assigning them is to attribute them to the three nearest-neighbor charge-compensation sites, C_{2v} Na^+ (110), C_{4v} Na^+ (200), and C_s Na^+ (211). The corresponding statistical weights are 12:6:24 (see Table I). Anticipating the site-selective excitation and emission results which will be presented in the future,¹⁶ we know that lines 1 and 2 contain most of the $4fG \rightarrow 5de$ oscillator strength for their respective sites, whereas lines 3 and 8 of comparable intensity originate from a third pair. Summing their intensities yields a ratio close to the purely statistical 12:6:24 prediction for the (110), (200), and (211) pairs. Their Boltzmann factors, calculated using $u_i/kT_d = -3.04/m$, would be 72:21:12. Although these factors

TABLE III. Summary of prominent laser-excitation peaks of sample 4, Ce:Na:CaF₂. Data tabulated are from both the crystal zone exhibiting C_{4v} F⁻(100) and C_{3v} F⁻(111) site peaks (the corresponding spectrum is in Fig. 6), and the crystal zone exhibiting an absence of F⁻ peaks [the corresponding spectra are in Figs. 5(a)–5(c)]. Δ₀ is the separation of the C_{4v} F⁻(100) center's vibrational bands from the origin. Vibration is abbreviated as *v*, *w* denotes a weak line, *h* denotes a hot band. Possible assignments for some Na⁺ lines are listed. Line association to sites labeled *A, B, C, . . .* is based on site-selective results (Ref. 16).

Assignment	Vacuum $\bar{\nu}$ (cm ⁻¹)	Linewidth FWHM (cm ⁻¹)	Δ ₀ (cm ⁻¹)
C _{4v} F ⁻ (100)	31 922.2	2.0	0
C _{4v} F ⁻ (100)+ <i>v</i>	32 022		100
C _{3v} F ⁻ (111)	32 027		
C _{3v} F ⁻ (111)	32 057.4	2.5	
C _{3v} F ⁻ (111)	32 058.8		
C _{4v} F ⁻ (100)+ <i>v</i>	32 090		168
C _{4v} F ⁻ (100)+ <i>v</i>	32 118		196
C _{4v} F ⁻ (100)+ <i>v</i>	32 144		222
C _{4v} F ⁻ (100)+ <i>v</i>	32 156		234
zero-phonon line (not Na ⁺)	32 178.5	1.0	
zero-phonon line (not Na ⁺)	32 196.5	1.0	
Na ⁺ line 1 <i>h</i> (<i>a</i>), site <i>A</i> , C _{2v} (110)?	32 214		
Na ⁺ line, <i>w</i>	32 219.5		
C _{4v} F ⁻ (100)+ <i>v</i>	32 226		304
Na ⁺ line 1, site <i>A</i> , C _{2v} (110)?	32 227.8	1.1	
Na ⁺ line, <i>w</i>	32 235.6		
Na ⁺ line, <i>w</i>	32 237.9		
Na ⁺ line, <i>w</i>	32 241.8		
Na ⁺ line, <i>w</i>	32 252.1		
Na ⁺ line, <i>w</i>	32 254.0		
C _{4v} F ⁻ (100)+ <i>v</i>	32 254		332
Na ⁺ line 1 <i>h</i> (<i>b</i>), site <i>A</i> , C _{2v} (110)?	32 277	7	
Na ⁺ line 2 <i>h</i> , site <i>B</i> , <i>w</i> , C _{2v} (200)?	32 293.5	1.1	
Na ⁺ line 3 <i>h</i> , site <i>C</i> , C _s (211)?	32 296.0	1.1	
Na ⁺ line 2, site <i>B</i> , C _{4v} (200)?	32 298.5	1.2	
Na ⁺ line 3, site <i>C</i> , C _s (211)?	32 305.5	0.9	
Na ⁺ line	32 309.3		
Na ⁺ line	32 312.1		
Na ⁺ line	32 313.9		
Na ⁺ line	32 315.7		
Na ⁺ line 4, site <i>D</i>	32 317.0		
Na ⁺ line, shoulder	32 318.4		
Na ⁺ line 5(<i>a</i>)	32 320.4		
Na ⁺ line 5(<i>b</i>), 8 <i>h</i> , sites <i>B</i> and <i>C</i>	32 321.4		
Na ⁺ line	32 322.9		
Na ⁺ line 6, site <i>E</i>	32 323.5, 32 324.2		
spectral hole, O _h site	32 325.0		
Na ⁺ line 7	32 326.1, 32 327.1		
Na ⁺ line, shoulder	32 326.8		
Na ⁺ line	32 328.3		
Na ⁺ line 8, sites <i>C</i> and <i>D</i>	32 329.6		
Na ⁺ line 9	32 331.6	1.2	
Na ⁺ line 10 <i>h</i> , site <i>F</i>	32 334.2	1.0	
Na ⁺ line, <i>w</i>	32 335.1		
Na ⁺ line 10, site <i>F</i>	32 338.2	1.1	
Na ⁺ line 11, site <i>F</i>	32 343.6	0.7	
Na ⁺ line	32 344.9		
Na ⁺ line 12, site <i>F</i>	32 347.9	1.1	
Na ⁺ line 13	32 353.1	0.9	
C _{4v} F ⁻ (100)+ <i>v</i> (A _{1g})	32 408		486

spoil the good match somewhat, we cannot conclude anything without examining the transition probabilities. At least this initial assignment remains a reasonable one.

It is possible, however, to reconcile the total area under the distant pair region with that of the lines using the Coulomb potential and the resulting Boltzmann factors. The ratio of the narrow line area to the broad band around $32\,325\text{ cm}^{-1}$ seems to be about 1:1, and thus the two parts of the partition function should also be in this ratio; hence $\sum_i g_i \exp(u_i/kT) \approx 13\,000$. Taking a crude average, $\exp(-u_i/kT) = 13\,000/446 = 29.1$, and $u/kT = -3.4$. This is in reasonable agreement with the Coulomb result using $\epsilon = 6.7$, of $-3.04/m$, given above. The apparent intensity ratios of lines 1, 2, and 3 are not, therefore, purely statistical. There appear to be fewer remote pairs than a statistical distribution indicates.

We have not made an accurate study of the spectral areas as yet and we do not want to push this line of investigation any further. But an interesting discovery has led to another estimate of the population of distant pair sites (O_h sites). This will be presented in the next section.

IV. EXCITATION SPECTRA OF THE $\text{Ce}^{3+}:\text{Na}^+:\text{CaF}_2$ CHARGE-COMPENSATION PAIRS AND OBSERVATION OF HOLE BURNING

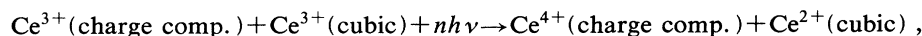
A. The $\text{Ce}^{3+}:\text{Na}^+$ pairs

Figure 5 shows laser-excitation spectra of the fast-cooled $\text{Ce}^{3+}:\text{Na}^+:\text{CaF}_2$ sample 4 taken at 1.8 and 15 K. The most prominent peaks are numbered starting at the lowest-energy Na^+ line at $32\,227.8\text{ cm}^{-1}$. The position and widths of these lines are listed in Table III (cm^{-1} units are vacuum-corrected values). This table also contains lines from other sites such as the $\text{F}^- C_{4v}(100)$ and the $\text{F}^- C_{3v}(111)$ which will be discussed later. Initially, the excitation spectrum [Fig. 5(a)] is quite similar to the absorption spectrum in Fig. 4(d), and exhibits all of the lines tabulated from the original photographic plates.³ It is worth pointing out that approximately two decades elapsed between these two measurements. Apparently the $\text{Ce}^{3+}:\text{Na}^+$ centers are quite thermally stable and persist for many years in CaF_2 . Note that small differences that exist between line energies and wavelengths of the

excitation spectra and those of the previously presented absorption spectra are due to a systematic error in the absorption calibration.³ The more accurate excitation values, tabulated in Table III, should be used. Later, high-resolution absorption spectra²³ of the codoped sample 4 agree to better than 1 cm^{-1} with the laser-excitation spectra.

After further excitation scans and an emission study in which most of the sharp lines were selectively irradiated, however, the spectrum changed [Figs. 5(b) and 5(c)]. A deep, sharp spectral hole appeared at $32\,325\text{ cm}^{-1}$, the energy of the uncompensated, O_h -center transition. The first laser spectrum taken of the sample, Fig. 5(a), exhibits a small notch (1.5% of the peak intensity) that might be the initial appearance of this feature. In addition, the intensities of the lines seem to have decreased relative to the central peaks flanking the hole. The hole persists through thermal cycling to room temperature, for a period of at least 2 weeks and perhaps longer. It is important to note that the hole at $32\,325\text{ cm}^{-1}$ appears while exciting nonresonantly. The laser was tuned into resonance with the zero-phonon lines well removed from $32\,325\text{ cm}^{-1}$ in order to study the site-selected emission spectra. Subsequently, the appearance of the spectral hole was noted.

The most likely explanation for the appearance of the spectral hole is that the charge-compensated Ce^{3+} centers photoionize with good efficiency under moderate-intensity uv laser excitation. Subsequently, the freed electron traps at uncompensated (O_h) Ce^{3+} centers, reducing them to Ce^{2+} and leaving a hole at $32\,325\text{ cm}^{-1}$. The observed hole is, therefore, an acceptor hole and reflects the disappearance of the trapping center in contrast to the more common, resonant, donor-hole-burning mechanism. The nonappearance of donor holes in the spectra must be explained by lack of laser resolution. Instead of holes, merely reductions in transition intensities of the photoionizing sites are observed in these samples [see Fig. 5(c)]. In excitation spectra of $\text{Ce}^{3+}:\text{Na}^+:\text{SrF}_2$ samples, donor-hole burning was observed in the inhomogeneously broadened line associated with the $C_{4v}\text{ F}^-(100)$ site. Notches in this 0-0 line appeared while the laser was set in resonance with it to take emission spectra (see Sec. V). An equation describing the photoionization and trapping process is



where n is the number of photons involved in ionizing the charge-compensated Ce^{3+} . The filled-shell Ce^{4+} is likely to be spectroscopically inactive in CaF_2 and SrF_2 ; however, the Ce^{2+} ion's spectroscopy is well understood, at least in CaF_2 .²⁴ Thus, an experiment to confirm the above mechanism by monitoring the Ce^{2+} product is feasible. This has not yet been attempted in the $\text{Ce}^{3+}:\text{Na}^+$ codoped crystals (however, this experiment has been successfully completed at room temperature for singly doped $\text{Ce}^{3+}:\text{CaF}_2$ samples,^{25,26} as discussed below).

Another possible explanation for the hole's appearance

is that Ce^{3+} O_h sites, themselves, are photoionized, leaving Ce^{4+} . This second explanation does not fit into the sequence of events leading to the hole's appearance, setting the laser in resonance with the lower-energy Na^+ lines for several hours during site-selective emission scans, followed by the appearance of the spectral hole at the O_h site's energy. A tunneling process in which the electron never enters the conduction band cannot be ruled out by our experiments. Such tunneling is expected to be negligible, however, since the centers involved are far removed from each other. Finally, another ground-

state process should be mentioned. A migration of excess interstitial F⁻ ions to pair with uncompensated Ce³⁺ O_h ions could occur, since the F⁻ ion is mobile in fluorite lattices at room temperature. This process is ruled out since the spectral hole at the Ce³⁺ O_h absorption energy did not occur until the sample was exposed to laser light. Earlier absorption measurements showed no hole.

Assuming the photoionization model to be correct, a striking feature of the observed spectral changes is the site selectivity of the trapping. The remotely compensated, cubic Ce³⁺ ion is a much more efficient electron trap than the Ce³⁺:Na⁺ pair sites. While a careful study of hole-burning efficiency has not been conducted, the cubic Ce³⁺ site is at least 20 times more efficient a trap than the various Ce³⁺:Na⁺ pairs based on line-intensity changes.

Closely related observations in Ce³⁺:CaF₂ singly doped samples have been reported very recently by Pogatshnik and Hamilton.^{25,26} These workers found that following room-temperature excitation of the 4*f* → 5*d* Ce³⁺ transition at 308 nm, bleaching of the broadband ultraviolet absorption spectrum of the Ce³⁺ C_{4*v*} F⁻(100) center and the production of the characteristic Ce²⁺ spectrum in the visible and near infrared occurs. This process was shown to have a stepwise two-photon mechanism^{25,26} through careful modeling of the power dependence. These authors report observation of the reverse process, the one-photon ionization of the Ce²⁺ product, as well. Photoconductivity signals were observed for both cases, exciting the Ce³⁺ and the Ce²⁺ bands, confirming that the electrons are excited into the conduction band.^{25,26} The photoconductivity of Ce²⁺ in CaF₂, SrF₂, and BaF₂ has been well characterized by Pedrini and co-workers.²⁷ These room-temperature results on the most common

Ce³⁺ site, the C_{4*v*} F⁻(100) center, strongly suggest that the same type of two-photon photoionization is responsible for the low-temperature spectral changes in the Ce³⁺, Na⁺ codoped CaF₂ crystals. Our high-resolution, low-temperature work unambiguously demonstrates the disappearance of remotely compensated, O_h Ce³⁺ sites when charge-compensated Ce³⁺ sites are excited. This is true in both CaF₂ and SrF₂ host crystals. This supports Pogatshnik and Hamilton's conclusion that O_h-symmetry Ce³⁺ sites are the electron traps in singly doped Ce³⁺:CaF₂.

The area of the spectral hole, i.e., the total amount of absorption lost in the 32 325-cm⁻¹ region, should be proportional to the number of distantly compensated ions. This provides another estimate of the part of the partition function due to these ions. From its appearance in Fig. 5 the area of the spectral hole gives an even smaller ratio than the estimate of the previous section.

Another difference between the 1.8- and 15-K spectra in Fig. 5 is the presence of hot bands at 32 227, 32 296.0, and 32 334.2 cm⁻¹, less obviously at 32 214 and 32 321.4 cm⁻¹, and possibly at 32 293.5 cm⁻¹. These are seen most clearly in Fig. 5(b) and are assigned to their parent bands with information from site-selective emission and excitation spectra that will be presented in a future paper. The hot bands are useful for determining ground-state ²F_{5/2} G energy-level splittings. Manthey also reported the observation of the first three hot bands.³

B. The F⁻(100) and F⁻(111) sites

Figure 6 shows a laser-excitation spectrum of a small (~200 μm²) zone near the edge of Ce³⁺:Na⁺:CaF₂ sam-

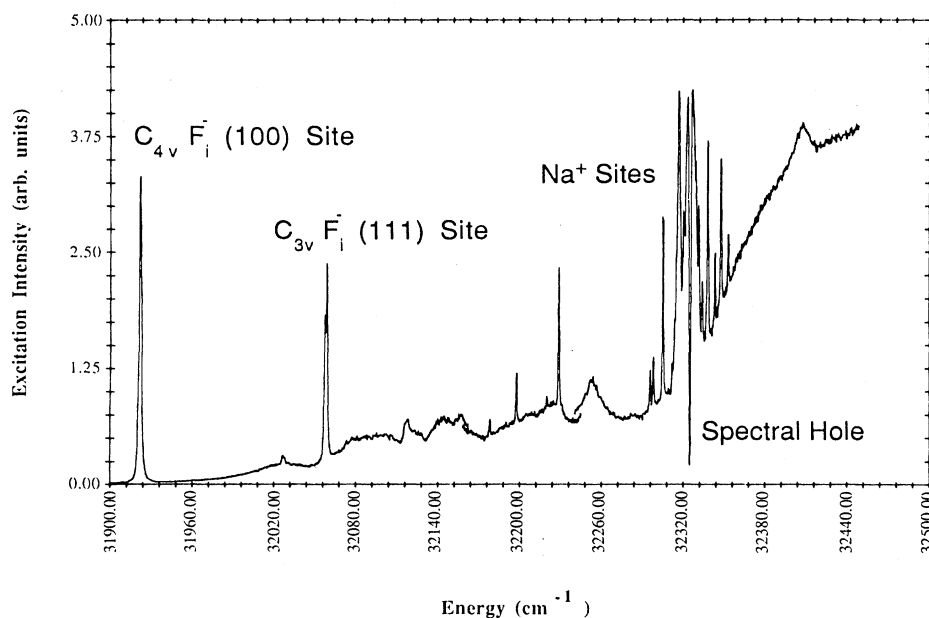


FIG. 6. High-resolution laser-excitation spectrum of sample 4, Ce³⁺:Na⁺:CaF₂. The spectrum is a composite of three overlapping scans. Spectrum of sample zone that exhibits zero-phonon lines of the C_{4*v*}-F⁻(100) and C_{3*v*} F⁻(111) sites as well as the numerous Na⁺ sites. Sample temperature is 15 K.

ple 4. This zone exhibited zero-phonon lines of interstitial fluoride-ion sites as well as the Na^+ lines shown in Fig. 5. The common tetragonal, C_{4v} $\text{F}^-(100)$ line at $31\,922\text{ cm}^{-1}$ and its vibronic sideband are prominent; the doublet due to the trigonal, C_{3v} $\text{F}^-(111)$ site at $32\,058\text{ cm}^{-1}$ is also seen. A hot band from the C_{3v} $\text{F}^-(111)$ site is also observed. These energies are tabulated in Table III and are in agreement with previously published values.^{1,2} Note that reduction of crystal-field symmetry from O_h to C_{3v} does not split the $5de$ level's degeneracy. The C_{3v} $\text{F}^-(111)$ transition is split by 1.4 cm^{-1} due to the

second-order effect of spin-orbit-coupling mixing of the $5de$ and $5dt$ states, combined with the reduction in symmetry.² More remotely compensated C_{3v} -symmetry centers such as $\text{Na}^+(222)$ will certainly have unresolvable splittings. The rising broad band to high energy of the Na^+ lines in Fig. 6 can be understood as the sum of the vibronic sidebands of the different zero-phonon lines. The only prominent feature in the broad band is the C_{4v} $\text{F}^-(100)$ site's 486-cm^{-1} , A_{1g} -type, one-quantum, vibrational level at $32\,408\text{ cm}^{-1}$. This spectrum was taken of a "fresh," nonirradiated region of the sample. The appear-

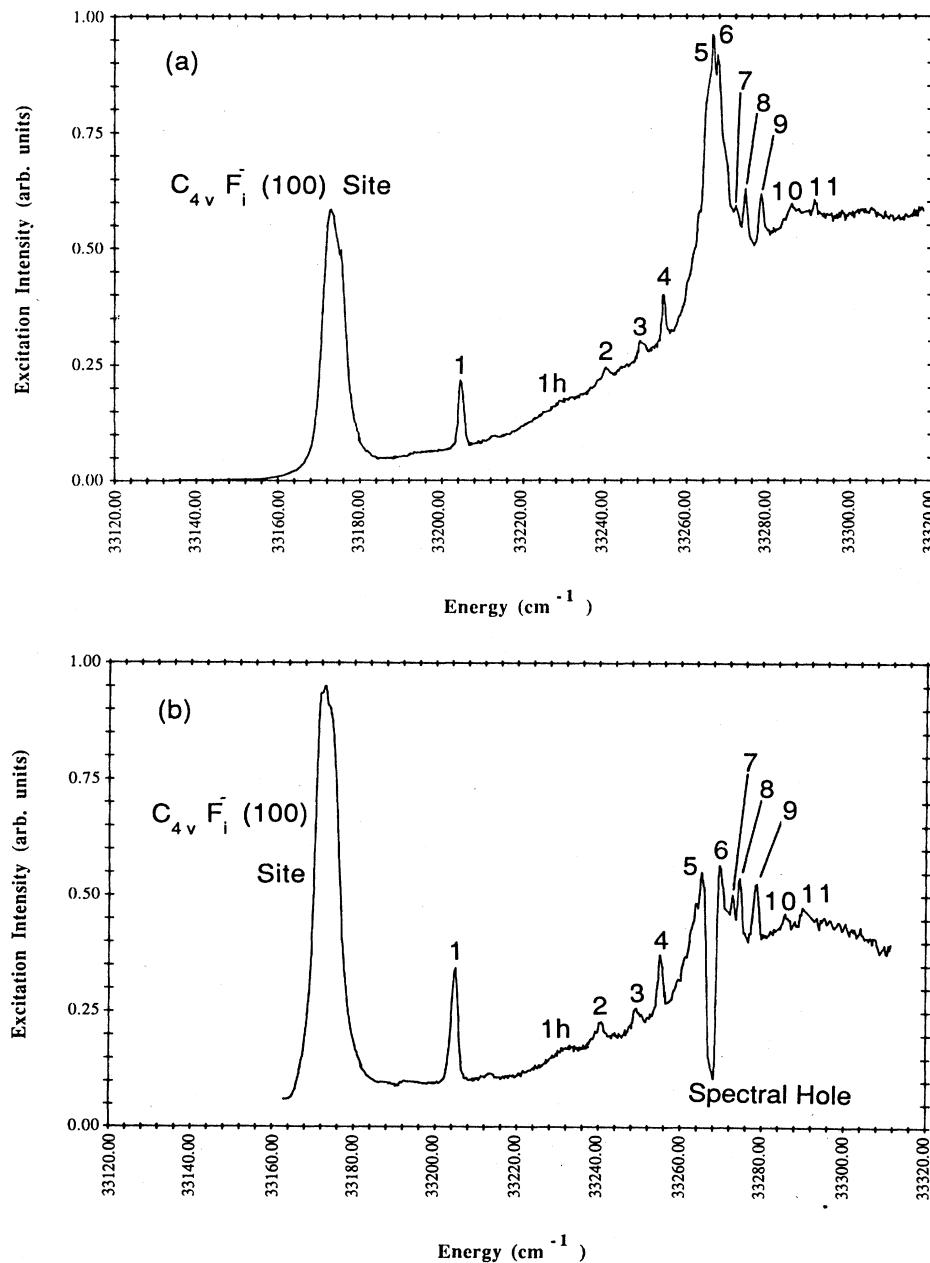


FIG. 7. High-resolution laser-excitation spectra of sample 5, $\text{Ce}^{3+}:\text{Na}^+:\text{SrF}_2$. Peak energies and features are listed in Table III. All numbered peaks are Na^+ sites. (a) Initial 15-K spectrum. (b) Later 15-K spectrum after extensive laser excitation of all prominent peaks. Note the appearance of a spectral hole at $33\,267\text{ cm}^{-1}$. (c) 1.8-K spectrum of different piece of same boule.

TABLE IV. Prominent laser-excitation peaks of Ce:Na:SrF₂ [the corresponding spectra are Figs. 7(a)–7(c)]. The notation is the same as Table III.

Assignment	Vacuum $\bar{\nu}$ (cm ⁻¹)	Linewidth FWHM (cm ⁻¹)
C _{4v} F ⁻ (100)	33 173	11, 7
Na ⁺ line	33 191	
Na ⁺ line	33 199	
Na ⁺ line 1, site A, C _{2v} (110)?	33 204.7	1.3
Na ⁺ line	33 212.4	
Na ⁺ line 1h, site A, C _{2v} (110)?	33 232	5
Na ⁺ line	33 238.8	
Na ⁺ line 2	33 240.1	1.3
Na ⁺ line 3	32 248.9	1.0
Na ⁺ line 4	33 254.4	1.5
Na ⁺ line	33 258.0	
Na ⁺ line	33 259.2	
Na ⁺ line	33 260.3	
Na ⁺ line 5(a)	33 262.2	
Na ⁺ line 5(b)	33 263.3	
Na ⁺ line 5(c)	33 265.1, 33 266.2	
spectral hole, O _h site	33 267.2	1.9
Na ⁺ line 6	33 270.0, 33 268	
Na ⁺ line 7	33 272.4	0.8
Na ⁺ line 8	33 274.3	1.3
Na ⁺ line 9	33 278.7	1.3
Na ⁺ line 10	33 286.3	
Na ⁺ line 11	33 291.6	

ance of the very deeply burned spectral hole at 32 325 cm⁻¹ in Fig. 6 could then be due to (a) photoionization of the low-energy sites during the course of the approximately 2-h scan, or (b) migration of electrons into this region of the crystal from the previously excited region ~2 mm away. Explanation (a), photoionization of the F⁻ sites, seems more likely. It is possible these sites lose an

electron more efficiently than Na⁺-compensated sites. It should be stressed that the bulk of Ce³⁺:Na⁺:CaF₂ sample 4 showed excitation spectra with no F⁻-site lines. It is likely that the observation of these lines in a small zone near the sample edge is due to the presence of the sites there at the time of growth and heat treatment two decades ago. Any slow movement towards thermodynamic

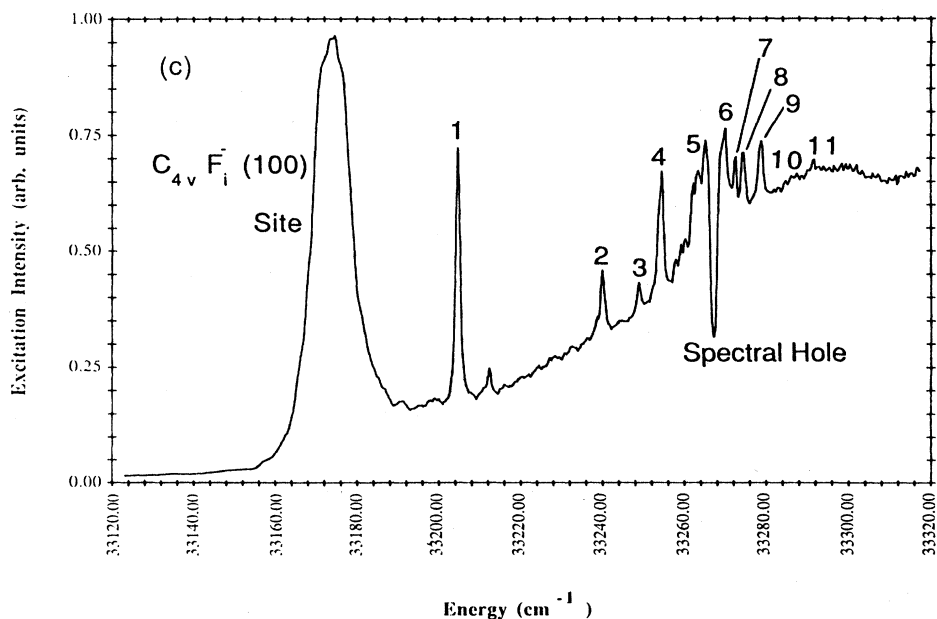


FIG. 7. (Continued).

equilibrium that might have occurred would be expected to affect the sample as a whole.

V. EXCITATION SPECTRA OF THE $Ce^{3+}:Na^+ :SrF_2$ CHARGE-COMPENSATION PAIRS

Optical results for $Ce^{3+}:Na^+$ centers in the SrF_2 host are now discussed. The excitation spectra of $Ce^{3+}:Na^+$ codoped SrF_2 crystals bear a strong resemblance to those of the previously discussed CaF_2 case. Both show ultraviolet lines from multiple $Ce^{3+}:Na^+$ pair sites, and after laser irradiation of these lines, both systems exhibit a deep spectral hole approximately in the center of the Na^+ line distribution. Figures 7(a)–7(c) show excitation scans at two different temperatures, 15 and 1.8 K. The Na^+ lines are numbered, and the major spectral features are listed in Table IV. The sample studied had not been heat treated, and the $C_{4v} F^-(100)$ peak centered at $33\,173\text{ cm}^{-1}$ is present in all the scans. No samples exhibiting isolated cubic lines, such as those shown in absorption in Figs. 4(a) and 4(b), have been studied for $Ce^{3+}:SrF_2$. Nevertheless, it seems fairly certain that the distant Na^+ site's transition energies will converge to the O_h value. In Fig. 7 this occurs at around $33\,267\text{ cm}^{-1}$, and at 1.8 K a deep spectral hole centered at $33\,267.2\text{ cm}^{-1}$ is seen in crystals subjected to laser excitation of the charge-compensated sites [see Fig. 7(b)]. In light of the results for the $Ce^{3+}:Na^+ :CaF_2$ samples, we conclude that $33\,267\text{ cm}^{-1}$ is the energy of the remotely compensated, O_h site. The lowest-energy Na^+ peak, line 1 at $33\,204.7\text{ cm}^{-1}$, is believed to be from the $C_{2v} Na^+(110)$ site. These three sites, $C_{4v} F^-(100)$, $C_{2v} Na^+(110)$, and cubic, are further

characterized through the site-selective emission and excitation work which will be presented in a future paper.

All of the transition energies of the SrF_2 sites are higher than those of their CaF_2 analogues. This is expected for Ce^{3+} in the weaker crystal field of the larger SrF_2 lattice, the shift going in the direction of the $5de$ energies. The axial crystal fields of the charge compensators are also weaker by virtue of the larger lattice constant, resulting in smaller splittings. This is evident in Fig. 7; the lines are more closely spaced than in CaF_2 . The shifts away from the cubic line energy are also smaller. One result of the weaker crystal field is that fewer sites are able to be characterized unambiguously due to spectral congestion.

One somewhat odd feature of the spectrum in Fig. 7 is the breadth of the $C_{4v} F^-(100)$ center's line at $33\,173\text{ cm}^{-1}$. With a FWHM linewidth of $11\text{--}7\text{ cm}^{-1}$ depending on the sample studied, it is broader than the other zero-phonon features. This line was observed at $33\,172\text{ cm}^{-1}$ by both Kaplyanskii and Manthey in singly doped samples, the latter author reporting a linewidth of 3 cm^{-1} . Inhomogeneous broadening, as opposed to experimental artifacts, is demonstrated to account for the linewidth. One manifestation of this is shown by monitoring the $C_{4v} F^-(100)$ site's emission while exciting at different energies within the line profile. The sharp emission line energies into the ${}^2F_{5/2}$ and ${}^2F_{7/2}$ manifolds are found to differ somewhat. When one of these energies is selectively monitored with the high-resolution monochromator, and the excitation spectrum scanned, a narrowed line profile is obtained. This is shown in Fig. 8 where the line has narrowed from 7.0 to 1.5 cm^{-1} FWHM. This

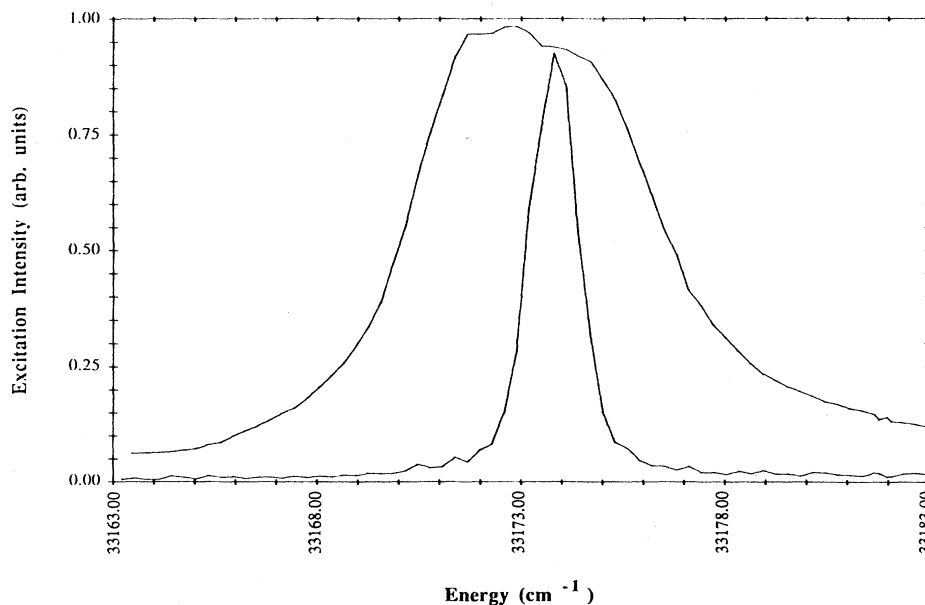


FIG. 8. Observation of excitation line narrowing in the broad $C_{4v} F^-(100)$ origin of the $Ce^{3+}:Na^+ :SrF_2$ sample. 6.5-cm^{-1} FWHM line is the broad-band-monitored excitation spectrum. 1.5-cm^{-1} FWHM is the selective excitation spectrum monitoring the sharp line ${}^2F_{7/2}$ emission at 322.50 nm only.

narrowing effect may be termed excitation line narrowing in analogy with the more frequently employed fluorescence line-narrowing experiment it mirrors. Obviously, not all of the inhomogeneous broadening is removed in Fig. 8, but it is reduced, with only the subset of centers emitting strongly at 322.50 nm appearing. The cause of the broadening remains in question. One possibility is that some clustering of the C_{4v} F⁻(100) pair centers occurs. This proven inhomogeneity must be borne in mind when the C_{4v} F⁻(100) emission results, which will be presented in a future paper are interpreted.

During the investigation of this broadened line, at various spots in the sample, spectral holes were burned in it. These appear as notches in the 33 173-cm⁻¹ excitation feature in Figs. 7(a)–7(c), most noticeably in Fig. 7(a) on the blue side of the peak of the approximately Gaussian 0-0 line. This provides clear evidence of the donor photoionization hole burning in these Ce³⁺-doped systems. The other charge-compensated lines, in both CaF₂ and SrF₂ hosts, were not inhomogeneously broadened enough for the holes to be observed with our approximately 0.7-cm⁻¹ laser linewidth. Instead, as mentioned earlier, reduction in line intensity resulted from long irradiation. The cubic-site acceptor holes appeared, of course, by virtue of the inhomogeneous broadening caused by increasingly remote Na⁺ charge compensators.

The only apparent hot band in Figs. 7(a) and 7(b) is the broad peak at 33 232 cm⁻¹, line 1h. As will be presented in a future paper, this is shown to be associated with the C_{2v} Na⁺(110) peak, line 1, in analogy with the unusual Ce³⁺:Na⁺:CaF₂ result. The nonobservation of other hot bands must be due to the burying of weak features in the vibronic sideband of the C_{4v} F⁻(100) peak, and to the overlap of these features with other site's zero-phonon lines. Also, the ground-state splitting in the weaker fields of the SrF₂ charge-compensator sites is expected to be less, perhaps requiring lower temperatures than 1.8 K to quench hot bands in the crowded spectral region around 33 267 cm⁻¹.

VI. CONCLUSIONS

A summary of the main results and conclusions of this work follows. Suggestions for further work are made.

(1) Multiple Ce³⁺:Na⁺ charge-compensated sites are readily produced by doping CaF₂ and SrF₂ with CeF₃ and an excess of NaF. The absorption lines of these sites are approximately centered at the uncompensated, cubic

site's energy. The pair sites with the closest charge compensation have the lowest transition energies. The charge-compensation sites observed appear to exhibit a perturbational trend, with the energy-level spacings of the more distant sites converging to the values for the cubic center. These Na⁺ sites predominate over the more common F⁻ sites in samples rapidly cooled from high temperatures and appear to be in a nearly random distribution. Presumably this will hold true for many other trivalent rare-earth systems. This gives one the ability to introduce multiple rare-earth sites, creating inhomogeneous broadening at will. The Ce³⁺:Na⁺ charge-compensated sites in CaF₂ and SrF₂ may be classified as one of the simpler members of an understudied type of impurity center, the heterovalent center. In the Ce³⁺:Na⁺ cases presented here, an optically active ion (Ce³⁺) was introduced to form multiple centers with an optically inactive ion (Na⁺). The Coulomb attraction of two optically active ions could be used to create impurity centers with novel optical, charge-transfer properties. Codoping fluorite-type hosts with an optically active monovalent species (such as Cu⁺) and trivalent rare-earth ions would be an obvious first step in this direction.

(2) The uncompensated, cubic Ce³⁺-site absorption line in CaF₂ and SrF₂ disappears under nonresonant laser excitation when other Ce³⁺ charge-compensated sites are excited. This is consistent with a mechanism in which the charge-compensated centers photoionize and the uncompensated centers act as efficient electron traps. Uncompensated trivalent rare-earth sites have been long thought to be electron traps in various studies. This seems to be explicitly demonstrated in the Ce³⁺:Na⁺:CaF₂ and Ce³⁺:Na⁺:SrF₂ impurity crystals. The advantage in the present work is the identification of the O_h site and its presence in the midst of an inhomogeneously broadened band so hole burning could be observed. This effect seems related to other observed Ce³⁺ solid-state photochemistry and photophysics^{25–28} and merits further study.

ACKNOWLEDGMENTS

This research was supported by the U.S. Department of Energy under Grant No. DE-FG02-84ER45146. Dr. Roman Czernuszewicz and Professor Tom Spiro are thanked for the timely loan of a Displex refrigeration system.

*Present address: Department of Chemistry, Stanford University, Stanford, CA 94305.

†Present address: Nashua Corporation, 44 Franklin Street, Nashua, N.H. 03061.

¹A. A. Kaplyanskii, V. N. Medvedev, and P. P. Feofilov, *Opt. Spektrosk.* **14**, 644 (1963) [*Opt. Spectrosc. (USSR)* **14**, 351 (1963)].

²William J. Manthey, *Phys. Rev.* **B 8**, 4086 (1973).

³William J. Manthey, Ph.D. thesis, University of Chicago, 1972.

⁴G. L. Walker and R. M. Mires, *Phys. Rev.* **B 21**, 1876 (1980).

⁵R. M. Mires and G. L. Walker, *Phys. Rev.* **B 33**, 3516 (1986).

⁶C. A. Freeth and G. D. Jones, *J. Phys.* **C 15**, 6833 (1982).

⁷I. T. Jacobs, G. D. Jones, K. Zdansky, and R. A. Satten, *Phys. Rev.* **B 3**, 2888 (1971).

⁸*Crystals with the Fluorite Structure*, edited by W. Hayes (Clarendon, Oxford, 1974).

⁹N. V. Starostin, P. F. Gruzdez, V. A. Ganin, and T. E. Chebotareva, *Opt. Spektrosk.* **35**, 476 (1973) [*Opt. Spectrosc. (USSR)* **35**, 277 (1973)].

¹⁰N. V. Starostin, A. K. Gerasyuk, and V. A. Ganin, *Opt. Spek-*

- trosk. **43**, 480 (1977) [Opt. Spectrosc. (USSR) **43**, 283 (1977)].
- ¹¹J. M. Baker, in *Crystals with the Fluorite Structure*, Ref. 8, and references therein.
- ¹²S. D. McLaughlan, Phys. Rev. **160**, 287 (1967).
- ¹³X. Zachariasen, as cited in C. Kittel, *Introduction to Solid State Physics* (Wiley, New York, 1956), Vol. 2, p. 81.
- ¹⁴F⁻ interstitial sites [(100), (111), (211), the odd sublattice] are indexed by $2m-1$: $h^2+k^2+l^2=2m-1=R^2$. These Diophantine equations have no solutions when $2m$ or $2m-1=4^b(8c+7)$, where b and c are any rational integers, so there are breaks in the indexes $n=1,2,3,\dots$ and $m=0,1,2,3,\dots$ such as $n=14,30,\dots$, and $m=4,8,12,16,\dots$. Following Ref. 21, the site symmetry h,k,l relationships are C_{4v} , $h\neq 0, k=l=0$; C_{3v} , $h=k=l\neq 0$; C_{2v} , $h=k\neq 0, l=0$, C_s , $h\neq k, l=0$, C_s , $h\neq k=l$ hkl all $\neq 0$. Sites of more than one symmetry, or equivalently multiple solutions of the diophantine sum of three squares, occur for $n=9,13,17,18,19,25,27,31,33,34,\dots$ and $m=5,9,13,14,17,21,25,29,33,35,\dots$. For further discussion, we see introductory number-theory texts, e.g., E. Grosswald, *Topics from the Theory of Numbers* (Birkhäuser, Boston, 1984), or R. A. Archibald, *An Introduction to the Theory of Numbers* (Merrill, Columbus, OH, 1970).
- ¹⁵R. Lang, Can. J. Res. Sec. A **13**, 1 (1935); **14**, 127 (1936).
- ¹⁶D. W. Pack and D. S. McClure (unpublished).
- ¹⁷D. W. Pack, Ph.D. thesis, Princeton University, 1987.
- ¹⁸E. Friedman and W. Loh, J. Chem. Phys. **33**, 1275 (1960).
- ¹⁹W. Hayes, M. C. K. Wiltshire, W. J. Manthey, and D. S. McClure, J. Phys. C **6**, L273 (1973).
- ²⁰M. Schlesinger and G. W. F. Drake, Can. J. Phys. **54**, (1976).
- ²¹F. K. Fong, in *Physics of Electrolytes*, edited by J. Hladik (Academic, London, 1972), Vol. I, pp. 79-126.
- ²²The acceptable accuracy of this spherical shell approximation for distant neighbors can be verified by a direct count of sites within a given radius.
- ²³William Needleman (unpublished).
- ²⁴R. C. Alig, Z. J. Kiss, J. P. Brown, and D. S. McClure, Phys. Rev. **186**, 276 (1969).
- ²⁵G. J. Pogatshnik and D. S. Hamilton, Phys. Rev. B **36**, 8251 (1987).
- ²⁶G. J. Pogatshnik, Ph.D. thesis, University of Connecticut, 1986.
- ²⁷C. Pedrini, P. O. Pagost, C. Madej, and D. S. McClure, J. Phys. (Paris) **42**, 323 (1980).
- ²⁸W. Hayes and D. L. Staebler, in *Crystals with the Fluorite Structure*, Ref. 8.